Inhibition of Dyrk1a attenuates type 1 diabetic cardiomyopathy via anti-ferroptosis

JUNJIAN CHEN[1*], WANYI ZHANG[1*], TAO HONG[2*], JUNSHENG WANG[1], CHUAN CHEN[1], YING ZHANG[1], MI HU[1], NING YOU[3] and JIETAO HUANG[1]

[1]Department of Cardiovascular Medicine, Chongqing Emergency Medical Center, Chongqing University Central Hospital, Chongqing 400014, P.R. China; [2]Department of Cardiology and Respiratory, The 927th Hospital of The People's Liberation Army Joint Logistics Support Force, Puer, Yunnan 650000, P.R. China; [3]Chongqing Emergency Medical Center, Chongqing University Central Hospital, Chongqing 400014, P.R. China

Received April 25, 2026; Accepted July 21, 2026

DOI: 10.3892/mmr.2026.13996

Abstract. Diabetic cardiomyopathy (DCM) is a major complication of type 1 diabetes mellitus (T1DM) with limited treatment options. Dyrk1a is involved in multiple diseases, comprising neurodegenerative disorders, cancer and diabetes. In addition, Dyrk1a is an emerging therapeutic target. Nonetheless, it remains ambiguous with regard to its role in T1DM-related DCM. The present study investigated the function and mechanisms of Dyrk1a in DCM. Experimental T1DM was induced through sequential low-dose streptozotocin administrations via intraperitoneal delivery. The investigation showed conspicuous cardiac upregulation of Dyrk1a protein expression in this T1DM murine model. Pharmacological intervention was performed by employing the Dyrk1a-targeting compound harmine, administered through oral gavage, which ameliorated cardiac dysfunction characteristic of DCM. This therapeutic efficacy was mechanistically linked to ferroptosis inhibition, which was established through harmine-mediated attenuation of pathological signatures, namely reduced malondialdehyde accumulation, enhanced glutathione bioavailability, as well as elevated expression of ferroptosis regulators SLC7A11 and GPX4. It is noteworthy that co-administration of the ferroptosis activator erastin nullified the cardioprotective properties of harmine. Together, these findings establish harmine as an effective modulator of ferroptosis pathways, conferring protection against hyperglycemia-induced cardiomyocyte injury. Dyrk1a inhibition enhances cardiac function in T1DM by reducing ferroptosis.

Correspondence to: Professor Ning You, Chongqing Emergency Medical Center, Chongqing University Central Hospital, 1 Jiankang Road, Yuzhong, Chongqing 400014, P.R. China
E-mail: youning9851111@163.com

Professor Jietao Huang, Department of Cardiovascular Medicine, Chongqing Emergency Medical Center, Chongqing University Central Hospital, 1 Jiankang Road, Yuzhong, Chongqing 400014, P.R. China
E-mail: jiethuang@163.com

*Contributed equally

Key words: type 1 diabetic cardiomyopathy, ferroptosis, Dyrk1a, harmine

Introduction

As a chronic noncommunicable metabolic disorder that affects health systems globally, diabetes poses considerable clinical challenges, with type 1 diabetes (T1DM) accounting for ~5-10% of all diabetes cases worldwide (1). Among various manifestations of T1DM, diabetic cardiomyopathy (DCM) stands out as a remarkable cardiovascular consequence, characterized by both diastolic and systolic dysfunction. This condition functions as a key factor influencing negative clinical outcomes, markedly contributing to the morbidity and mortality associated with T1DM (2). Notwithstanding extensive research efforts over a number of years involving both preclinical studies and clinical populations, a pivotal gap persists in the availability of effective management strategies for DCM.

DCM pathogenesis involves complex multifactorial mechanisms. As contemporary studies demonstrate, initiation of cellular demise accelerates diabetes-mediated cardiac deterioration. While apoptosis constitutes the primary documented cell death modality in DCM progression (3), its suppression yields only partial cardiomyocyte survival enhancement under hyperglycemic conditions (4). The potential contributions of alternative regulated non-apoptotic cell death pathways to DCM pathogenesis, particularly in T1DM contexts, remain predominantly uncharted. In T2DM, accrued glucose derivatives and lipids provoke cardiotoxicity through glucotoxic and lipotoxic effects, concurrently exacerbating oxidative stress via excessive reactive oxygen species (ROS) generation. As these elements represent fundamental DCM pathomechanisms, blocking deleterious lipid metabolites and their peroxidative cascades proves pivotal for the prevention of cardiomyocyte loss and the maintenance of myocardial functionality (5). Ferroptosis emerges from dysregulated metabolic-redox equilibrium and participates in diverse pathological signaling cascades (6,7). This process requires

abundant ROS and polyunsaturated fatty acids to initiate uncontrolled lipid peroxidation when iron (Fe^{2+}) concentrations escalate. This cascade generates phospholipid hydroperoxides, the terminal effectors of ferroptosis, ultimately executing cellular destruction. Nascent evidence tentatively associates ferroptosis with DCM etiology (8). Wang *et al* (9) verified ferroptosis activity in type 2 diabetic murine myocardium. As the authors' research findings suggest, liproxstatin-1-mediated inhibition attenuated diastolic impairment. Parallel investigations in streptozotocin-induced T1DM rodents subjected to myocardial ischemia/reperfusion (MI/R) injury revealed intensified ferroptosis in diabetic hearts compared with controls. Ferrostatin-1 administration notably mitigated MI/R damage in DCM models (10). Notwithstanding the fact that ferroptosis has captured extensive attention, it remains incomplete about the current understanding of its regulatory mechanisms.

As a member of the dual-specificity tyrosine-regulated kinase family, Dyrk1a has been reported to perform irreplaceable roles in various diseases. Nevertheless, the potential intersection between Dyrk1a signaling and ferroptosis mechanisms remains poorly explored in current scientific literature. The CMGC kinase superfamily encompasses dual-specificity tyrosine-regulated kinases (Dyrk1a, Dyrk1b, Dyrk2, Dyrk3 and Dyrk4) alongside related enzymes encompassing CLKs, CDKs, MAP kinases and GSKs (11). These regulatory proteins orchestrate diverse cellular operations, spanning signal transduction, genomic stability maintenance, viability control and proliferative regulation (12). Notably, glycogen synthase kinase-3β (GSK-3β) functions as a pro-ferroptosis modulator through iron homeostasis governance (13), with recent evidence implicating it in MI/R-associated ferroptosis pathways (14). Within this kinase hierarchy, Dyrk1a modulates cardiomyocyte cell cycle dynamics (15). As validated by experimental evidence, either genetic ablation or pharmacological inhibition of Dyrk1a reactivates postnatal cardiomyocyte cycling, which thus enhances functional recovery following myocardial infarction in adult murine models (16,17). As accumulating evidence suggests, DYRK1A is involved in multiple diseases, such as neurological disorders, types of cancer and diabetes (18). Given its established involvement in diabetes, neuronal disease and types of cancer, alongside its emerging roles in cardiac repair, Dyrk1a represents a compelling candidate for exploring novel pathogenic mechanisms in diabetic cardiomyopathy. Nevertheless, the potential intersection between Dyrk1a signaling and ferroptosis mechanisms in the context of T1DM-induced cardiac injury remains entirely unexplored in current scientific literature. In this context, the present study developed a model of cell injury triggered by elevated glucose levels, alongside a mouse model of type 1 diabetic cardiomyopathy, to evaluate the impact of Dyrk1a on ferroptosis.

Materials and methods

Animals. A total of 24 male C57BL/6J mice (8 weeks old; 20-25 g) were sourced from Beijing Vital River Laboratory Animal Technology Co., Ltd. and housed under controlled environmental conditions, including a constant ambient temperature of 23±1˚C, relative humidity of 40-70% and a standardized 12-h light/dark cycle. Experimental diabetes induction was performed via five daily intraperitoneal administrations of streptozotocin (STZ; MedChemExpress) at a 50 mg/kg dosage, following established protocols (19). Control subjects received citrate buffer vehicle injections of an identical volume. At the 14-day post-induction interval, animals underwent 12-h fasting prior to diagnostic blood collection from caudal vessels; diabetes confirmation required fasting glucose concentrations exceeding 16.7 mmol/l (20). The mice were subsequently maintained under diabetic conditions for an additional 12 weeks before echocardiography and terminal tissue collection. With reference to pharmacological intervention, harmine (MedChemExpress) was administered by oral gavage at 12.5 mg/kg/day for 12 weeks. Erastin (MedChemExpress) was administered intraperitoneally at 40 mg/kg/day for 3 consecutive days during the indicated experimental period. Distilled water served as the vehicle for both compounds and control mice received equal volumes of vehicle (Fig. 1A). Longitudinal biometric surveillance included weekly evaluations of body mass and glycemic parameters through serial tail-vein phlebotomy. Terminal procedures employed sodium pentobarbital euthanasia (100 mg/kg, i.p.) with subsequent cardiac tissue procurement for analytical purposes. All protocols received prior endorsement from the Institutional Animal Care and Use Committee of Chongqing University (approval no. 2505001), with strict adherence to the NIH Guide for the Care and Use of Laboratory Animals (8th edition, 2011; http://grants.nih.gov/grants/olaw/guide-for-the-care-and-use-of-laboratory-animals.pdf) throughout the experimental timeline.

Echocardiography. Cardiac functional assessment used the Vevo 2100 high-frequency ultrasound platform (FUJIFILM VisualSonics). Isoflurane (3% for induction; 1.5% for maintenance, mixed with 98.5% oxygen) was used to anesthetize the mice before supine positioning on thermostatic pads maintaining core temperature at 37˚C. M-mode systolic parameters, encompassing left ventricular ejection fraction (LVEF) and left ventricular fractional shortening (LVFS), were quantified in the parasternal long-axis orientation, with analytical processing executed through Vevo LAB software (v5.5.1; FUJIFILM VisualSonics). Metric derivation underwent ≥3 successive cardiac cycles on average. Echocardiographic analyses were conducted by personnel blinded to therapeutic interventions.

Histological evaluation. Cardiac tissues underwent immediate perfusion with ice-cold phosphate-buffered saline (4˚C) followed by 24-h fixation in 4% paraformaldehyde at room temperature. Sequential dehydration through graded ethanol solutions preceded paraffin embedding and microtome sectioning at 4 μm thickness. Sections were stained with hematoxylin-eosin (H&E) at room temperature for 5 min with hematoxylin and 2 min with eosin according to the manufacturer's protocol (Beijing Solarbio Science & Technology Co., Ltd.). Fibrosis quantification employed Masson's trichrome methodology (Beijing Solarbio Science & Technology Co., Ltd.) at room temperature, with precise incubation intervals: Hematoxylin (10 min), ferric oxide (5 min), acid fuchsin (10 min), phosphomolybdate (10 min) and acetic acid (1 min).

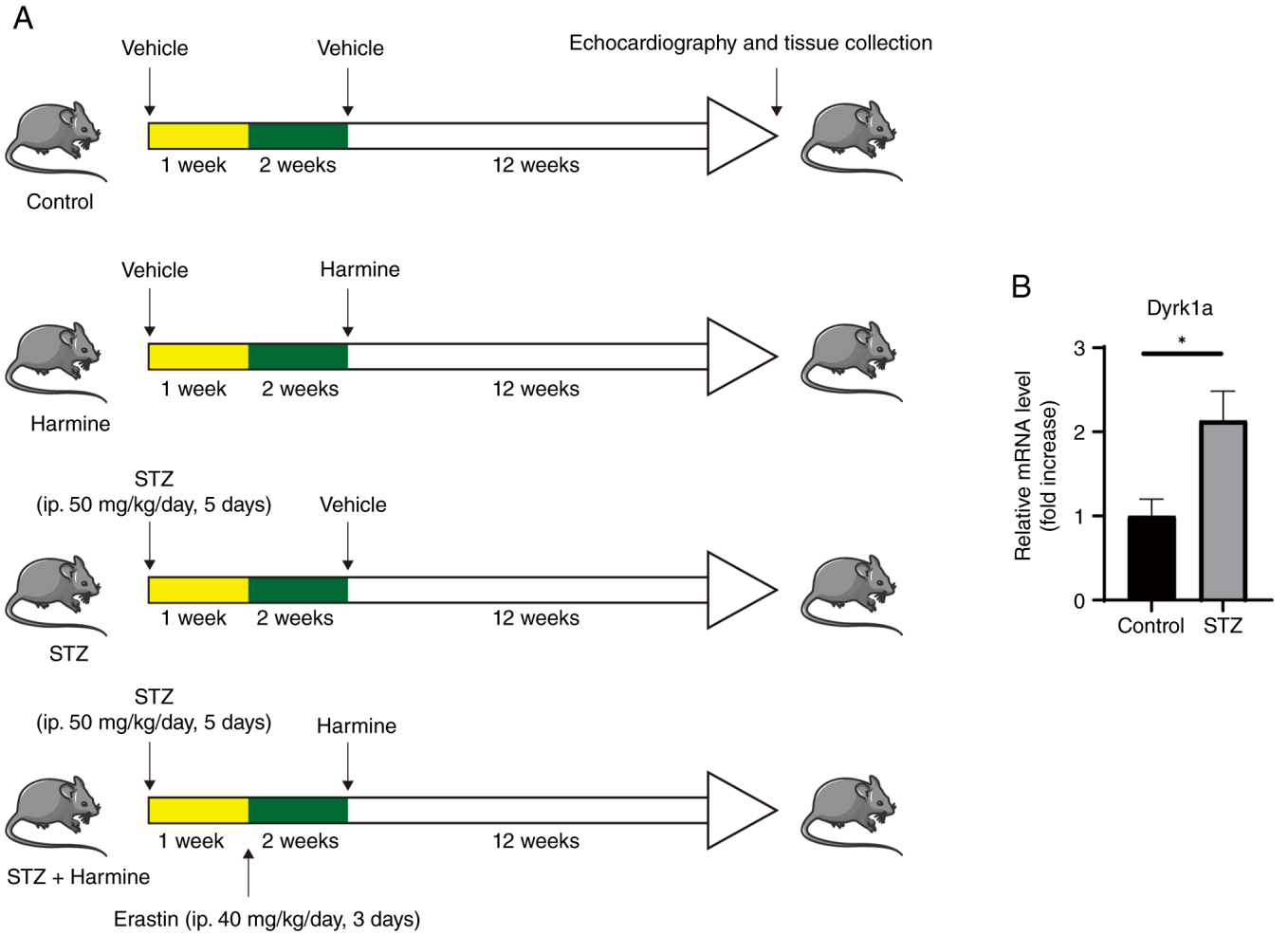

Figure 1. The expression of Dyrk1a was increased in the heart of type 1 diabetic mice. (A) Schematic diagram showing the treatments of the mice. (B) Reverse transcription-quantitative PCR was applied to assess the mRNA levels of Dyrk1a in type 1 diabetic mice (n=6 per group). Data are expressed as the mean ± SD. Student's t-test. *P<0.05. STZ, streptozotocin.

Digital imaging was conducted by using an Olympus VS200 slide-scanning platform (Olympus Corporation), while collagen deposition was calculated as fibrotic area percentage relative to total tissue area by employing ImageJ morphometry. Histomorphological assessment was performed in six randomized high-power fields (magnification, x400).

Enzyme-linked immunosorbent assay. Following sodium pentobarbital anesthesia, murine blood specimens were obtained via retro-orbital venous plexus puncture. Serum isolation involved centrifugation (3,000 x g, 20 min, 4˚C) for subsequent cytokine quantification. TNF-α and IL-6 concentrations were determined by utilizing commercial ELISA kits (Nanjing SenBeiJia Biological Technology Co., Ltd.; TNF-α, cat. no. SBJ-M0030; IL-6, cat. no. SBJ-M0657). For cardiac and cellular lipid peroxidation assessment, samples underwent homogenization in protease-inhibited ice-cold lysis buffer, with supernatants harvested post-centrifugation (1,200 x g; 4˚C; 10 min). Malondialdehyde (MDA) content was analyzed by employing specialized assay kits (Nanjing Jiancheng Bioengineering Institute), while cardiac lipid peroxide (LPO) quantification followed manufacturer protocols (Shanghai Enzyme-linked Biotechnology Co., Ltd.), comprising standardized well assays with 450 nm spectrophotometry. Reduced glutathione (GSH) and oxidized glutathione (GSSG) were evaluated fluorometrically (Beyotime Biotechnology) subsequent to tissue homogenization in Reagent M and ultracentrifugation (10,000 x g; 4˚C; 10 min) to collect assay-ready supernatants.

Transmission electron microscopy (TEM). Prior to secondary fixation, cardiac specimens underwent initial fixation by employing 1% osmium tetroxide in 3% glutaraldehyde. Subsequent dehydration employed progressively concentrated acetone solutions, followed by prolonged Epon 812 resin infiltration prior to polymerization embedding. Semithin sections received methylene blue staining, whereas ultrathin sections generated via diamond-knife microtomy were contrasted sequentially with uranyl acetate and lead citrate solutions. Ultrastructural analysis was conducted utilizing a JEM-1400FLASH (JEOL, Ltd.) transmission electron microscope.

Cell culture and cell viability assays. Primary ventricular cardiomyocytes were isolated from 1-3 day-old Sprague-Dawley neonates (n=20; Beijing Vital River

Laboratory Animal Technology Co., Ltd.) under controlled conditions at 22±2˚C, with a 12-h light/dark cycle and relative humidity of 40-60% (21). The neonates underwent isoflurane anesthesia followed by immediate euthanasia via cervical dislocation prior to cardiac excision. Harvested hearts underwent immediate immersion in pre-chilled ADS buffer (120 mmol/l NaCl, 20 mmol/l HEPES, 8 mmol/l NaH_2PO_4, 6 mmol/l glucose, 5 mmol/l KCl, 0.8 mmol/l $MgSO_4$, pH 7.4), followed by transferring them to fresh ADS and mechanical fragmentation into sub-1-mm^3 segments using scissors. Tissue fragments received iterative sterile ADS rinsing until effluent clarification. Digestive processing commenced with collagenase II solution (2 ml) and ADS (2 ml) in sterile 25-ml vessels under continuous 180 rpm agitation at 37˚C for 8 min. Resultant suspensions underwent ice-cooled filtration into 50 ml centrifuge tubes, supplemented with 1 ml fetal bovine serum (FBS; Gibco; Thermo Fisher Scientific, Inc.). Post-centrifugation (2,000 x g; 5 min at room temperature), supernatants were discarded and pellets resuspended in FBS for Petri dish plating. Subsequent 37˚C incubation under 5% CO_2 for 2 h facilitated cardiomyocyte-fibroblast segregation. Supernatant transfer to fresh 50 ml tubes enabled Percoll gradient purification (MilliporeSigma) in sterile ADS. In the aftermath of isolation via 1,800 x g centrifugation (45 min at room temperature) and initial 24-h culture in DMEM with 10% FBS/1% penicillin-streptomycin (37˚C/5% CO_2), cardiomyocytes were subjected to an *in vitro* DCM model protocol comprising sequential incubation: 16 h in 10% FBS-supplemented DMEM containing 5.5 mmol/l glucose, followed by 24 h in high-glucose (35 mmol/l) medium (22).

Cells were cultured in 96-well plates at a density of $5x10^3$ cells per well. Then, cell viability was assessed by employing a commercial CCK-8 kit (MedChemExpress) in line with the manufacturer's guidelines.

Determination of ROS generation. To measure intracellular ROS levels in primary cardiomyocytes, the cells were treated as indicated and subsequently incubated with DCFH-DA (10 μmol/l; Beyotime Biotechnology) or MitoSOX Red (5 μmol/l, MedChemExpress) for 30 min at 37˚C in the dark. Fluorescence detection was performed by utilizing a confocal laser scanning microscope (Olympus Corporation). The fluorescence intensity across the various groups was assessed by employing ImageJ (version 1.52, National Institutes of Health).

Western blotting. Western blotting was conducted to quantify protein abundance in myocardial tissue and isolated cardiomyocyte cultures. Subsequent to protein extraction with RIPA lysis buffer (Beyotime Biotechnology), lysate concentrations were determined with a BCA quantification kit (Beijing Solarbio Science & Technology Co., Ltd.; cat. no. PC0020). Aliquots (50 μg) underwent electrophoretic separation via SDS-PAGE on 10% gels and electrotransfer onto nitrocellulose membranes (Cytiva). After 60-min blocking at room temperature in 5% skimmed milk, membranes received overnight incubation (4˚C) with primary antibodies: anti-SLC7A11 (Invitrogen; Thermo Fisher Scientific, Inc.; rabbit; cat. no. 23657-RBM3-P1ABX; 1:1,000), anti-GPX4 (Proteintech Group, Inc.; rabbit; cat. no. 67763-1-Ig; 1:1,000) and GAPDH-specific antibody (Proteintech Group, Inc.; cat. no. 10494-1-AP, 1:10,000). Post-wash, HRP-conjugated secondary antibody (Thermo Fisher Scientific, Inc.; cat. no. C31460100) was applied for 1 h at room temperature, with signal development by employing an enhanced chemiluminescence (ECL) substrate (Thermo Fisher Scientific, Inc.; cat. no. 34577). Semi-quantitative analysis was performed using ImageJ (version 1.52, National Institutes of Health).

Reverse transcription-quantitative (RT-q) PCR. Cardiac tissue RNA extraction was performed with RNAiso Plus reagent (Takara Biotechnology Co., Ltd.) following the supplier's protocols. cDNA synthesis and qPCR were performed according to the manufacturer's protocols using SYBR Premix Ex Taq II (Takara Biotechnology Co., Ltd.) on a 7900HT Fast Real-Time PCR platform (Applied Biosystems; Thermo Fisher Scientific, Inc.) for specific mRNA quantification. qPCR was performed using a three-step protocol: 95˚C for 10 min; 35 cycles of 95˚C for 15 sec, 60˚C for 15 sec and 72˚C for 45 sec; then 72˚C for 7 min. GAPDH served as the normalization standard across triplicate reactions, and relative expression was calculated using the $2^{-\Delta\Delta Cq}$ method (23). Primer sequences are detailed in Table SI.

Seahorse respirometry. The Seahorse XFe24 Extracellular Flux Analyzer, along with Seahorse XF24 FluxPaks (Agilent Technologies, Inc.), was employed for respirometry analysis of seahorses. With an aim to determine oxygen consumption rates (OCR), primary cardiomyocytes were cultured in an assay microplate at a density of $4x10^4$ cells per well by utilizing growth medium. In the aftermath of treatment with specified reagents for the designated duration, the culture medium was substituted with Seahorse XF DMEM buffer. The OCR was measured both at baseline and after metabolic disturbances induced by 1.5 μmol/l oligomycin, 1 μmol/l FCCP (a mitochondrial uncoupler) and 0.5 μmol/l rotenone paired with antimycin A. Calculations were carried out by employing the Agilent Seahorse Wave Software designed for Agilent Seahorse XF analyzers (Agilent Technologies, Inc.).

Statistical analysis. The results were expressed as the mean ± SD. Statistical analyses were performed by using GraphPad Prism 9.0 (Dotmatics). Each experiment was independently repeated at least three times, with sample sizes and technical replicates specified in the corresponding figure legends. The Brown-Forsythe test was employed to assess homogeneity of variance among groups. One-way analysis of variance was performed for making comparisons among >2 groups, followed by Dunnett's post hoc test for comparisons against a single control group or Tukey's post hoc test for multiple pairwise comparisons when it was essential. Subsequently, a two-tailed unpaired Student's t-test was used for comparisons between two groups. Survival analysis was performed by employing the Kaplan-Meier method, with group differences assessed by the log-rank test. $P<0.05$ was considered to indicate a statistically significant difference.

Results

Inhibition of Dyrk1a improves cardiac function and ameliorates cardiac remodeling in STZ-induced type 1 diabetes.

Successful establishment of a T1DM model was confirmed in 8-week-old C57BL/6J mice following five consecutive days of intraperitoneal STZ injections (50 mg/kg/day), evidenced by fasting serum glucose >16.7 mmol/l (Figs. 1A and S1A). In an effort to investigate Dyrk1a's role in T1DM pathology, the present study analyzed cardiac Dyrk1a levels. Transcriptional analysis presented conspicuous upregulation of cardiac Dyrk1a 15 weeks post-STZ induction (Fig. 1B). In line with multiple findings from other studies (24-26), mice treated with STZ exhibited compromised cardiac function, which was improved (LVEF and LVFS; Fig. 2A) by using Dyrk1a inhibitors (Harmine; 12.5 mg/kg/day) and administering them intragastrically on a daily basis over a period of 12 weeks. In agreement with previous studies (27,28), mice with STZ-induced T1DM exhibited biochemical alterations and characteristic morphological changes, such as elevated serum concentrations of inflammatory markers (TNF-α and IL-6; Fig. 2B-D), along with disorganized myofibrils and cardiac fibrosis (Fig. 2D and E). Nevertheless, the administration of harmine improved or corrected these aforementioned abnormalities, encompassing both the biochemical aspects and the morphological (Fig. 2B-E).

Dyrk1a inhibition ameliorates ferroptosis in type 1 diabetic mice. Ferroptosis represents a critically implicated pathological pathway in DCM development within T2DM murine models (9,29,30). With an aim to investigate its potential involvement in T1DM pathogenesis, the present study initially quantified key biomarkers of lipid peroxidation, comprising MDA, LPO, GSH and the GSH/GSSG redox ratio, in cardiac tissue. As demonstrated by the data, STZ-induced T1DM mice manifested markedly elevated MDA and LPO concentrations concurrent with diminished GSH levels and suppressed GSH/GSSG ratios (Fig. 3A-D). In particular, harmine administration substantially attenuated these pathological deviations, restoring biomarker profiles without inducing remarkable alterations in control groups.

Further mechanistic analysis revealed substantial downregulation of cardinal ferroptosis regulatory proteins, particularly SLC7A11 and GPX4, in diabetic myocardial tissue (Fig. 3E). This pathological protein suppression was markedly attenuated subsequent to harmine intervention. Given mitochondria's established role in cellular defense against ferroptosis cell death (31,32), the present study conducted ultrastructural examination via TEM. Diabetic cardiomyocytes exhibited classical ferroptosis mitochondrial phenotypes (33), characterized by pronounced organelle shrinkage with markedly increased membrane electron density. It is pivotal to note that harmine treatment substantially mitigated these pathological ultrastructural alterations (Fig. 3F).

Ferroptosis inducer reverses harmine-mediated cardioprotection in diabetic cardiomyopathy. To further elucidate the mechanistic contribution of ferroptosis to harmine-mediated cardioprotection in type 1 DCM, the present study administered the canonical ferroptosis inducer erastin (40 mg/kg/day intraperitoneally for 3 consecutive days) to STZ-induced diabetic mice. Harmine intervention demonstrated substantial therapeutic efficacy in diabetic cohorts, manifesting as improved cardiac functional indices (Fig. 4A), attenuated serum elevations of pro-inflammatory biomarkers (Fig. 4B-C) and amelioration of myocardial histopathological abnormalities encompassing reduced interstitial collagen deposition (Fig. 4D). In particular, erastin co-administration not only potentiated diabetes-associated cardiac injury severity but also critically abrogated harmine's protective effects across all evaluated parameters, encompassing functional, inflammatory and structural metrics (Fig. 4). As collectively demonstrated by these pharmacological perturbation experiments, targeted induction of ferroptosis effectively neutralizes harmine's cardioprotective actions, thereby establishing ferroptosis pathway modulation as the fundamental mechanistic basis for harmine's therapeutic activity against experimental DCM pathogenesis.

Harmine attenuates high glucose-induced cardiomyocyte injury and ferroptosis. To decipher the molecular underpinnings of harmine-afforded cardioprotection, the present study systematically evaluated ferroptosis modulation in primary cardiomyocytes subjected to diabetic-mimetic high-glucose (HG) conditions (35 mmol/l). As evidently demonstrated by quantitative assessments, HG exposure markedly compromised cellular viability, an effect that was dose-dependently mitigated by harmine co-administration across a pharmacological range (10-50 μmol/l; Fig. 5A). Pathological profiling identified characteristic ferroptosis responses encompassing elevated MDA production signifying lipid peroxidation (Fig. 5B), depletion of GSH pools (Fig. 5C), diminished GSH/GSSG redox capacity (Fig. 5D) and suppressed expression of ferroptosis gatekeepers SLC7A11 and GPX4 (Fig. 5E). These perturbations occurred concomitantly with ROS accumulation (Fig. 5F-G). In addition, the present study employed extracellular flux analysis to assess mitochondrial respiratory capacity *in vitro* in real-time. HG markedly diminished the mitochondrial oxygen consumption rate (OCR) as well as both basal and maximal respiration (Fig. 5H). Therapeutic intervention with harmine (25 μmol/l) substantially counteracted these pathogenic shifts, demonstrating substantial attenuation of oxidative stress markers and restoration toward physiological levels across all quantified ferroptosis parameters (Fig. 5B-H).

Discussion

Cardiac physiology fundamentally rests with iron homeostasis, an essential trace element governing vital processes comprising metabolic regulation and bioenergetics (29). Disruption of this equilibrium manifests pathologically when redox-active iron species accumulate within cardiomyocytes, infiltrating mitochondria to execute oxidative damage that precipitates cardiac disorders (34). It is paramount to mention that research identifies ferroptosis, characterized by iron-dependent, unrestricted accrual of lethal phospholipid peroxides (6), as the primary driver of iron overload-induced cardiomyopathy (35). Emerging evidence positions ferroptosis as a paramount pathogenic factor across cardiovascular pathologies. Notably, ferroptosis inhibitors (vitamin E and coenzyme Q10) confer myocardial protection in diabetic models by mitigating oxidative stress (36,37), suggesting their particular relevance in DCM pathogenesis. Currently, direct mechanistic links

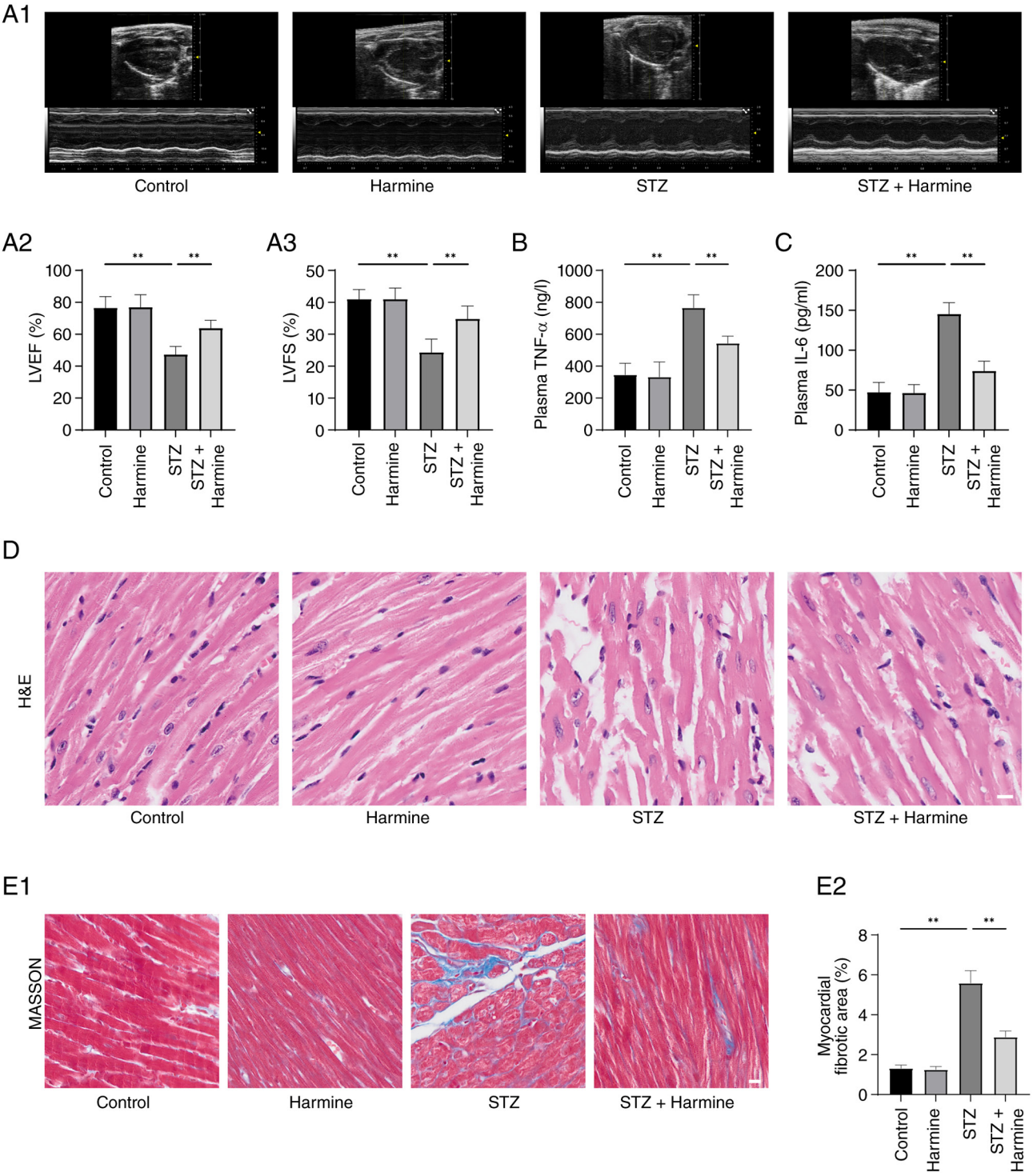

Figure 2. Inhibition of Dyrk1a improves cardiac function and ameliorates cardiac remodeling in type 1 diabetic mice. Mice received a treatment of STZ for a period of 5 days to trigger diabetic cardiomyopathy; the control group consisted of mice that were injected with a vehicle instead of STZ. After this, both the control and diabetic mice were given Harmine (12.5 mg/kg/day) or a vehicle via intragastric administration for 12 consecutive weeks. (A) Cardiac function was evaluated by echocardiography, comprising (A1) representative M-mode imaging, (A2) left ventricular ejection fraction (LVEF%) and (A3) left ventricular fractional shortening (LVFS%; n=6 for each group). The serum levels of biomarkers associated with inflammation, encompassing (B) TNF-α and (C) IL-6 were presented (n=6 for each group). (D) For evaluating myocardial injury, H&E staining was employed. Scale bar, 10 μm. (E) The presence of myocardial fibrosis is highlighted by Masson's trichrome staining, which encompasses (E1) representative images as well as (E2) quantification of the fibrotic areas. Scale bar, 10 μm (n=6 for each group). Data are mean ± SD. **P<0.01. Data were analyzed by employing one-way ANOVA followed by Dunnett's post hoc test. STZ, streptozotocin; LVEF, left ventricular ejection fraction; LVFS, left ventricular fractional shortening; TNF-α, tumor necrosis factor-α; IL-6, interleukin-6; H&E, hematoxylin and eosin.

have confirmed ferroptosis involvement in DCM progression, though precise regulatory networks remain elusive. Experimental models reveal stage-dependent divergence. To be specific, despite the fact that apoptosis predominates in early DCM phases before diminishing (38), ferroptosis emerges as a critical mediator during advanced disease (9).

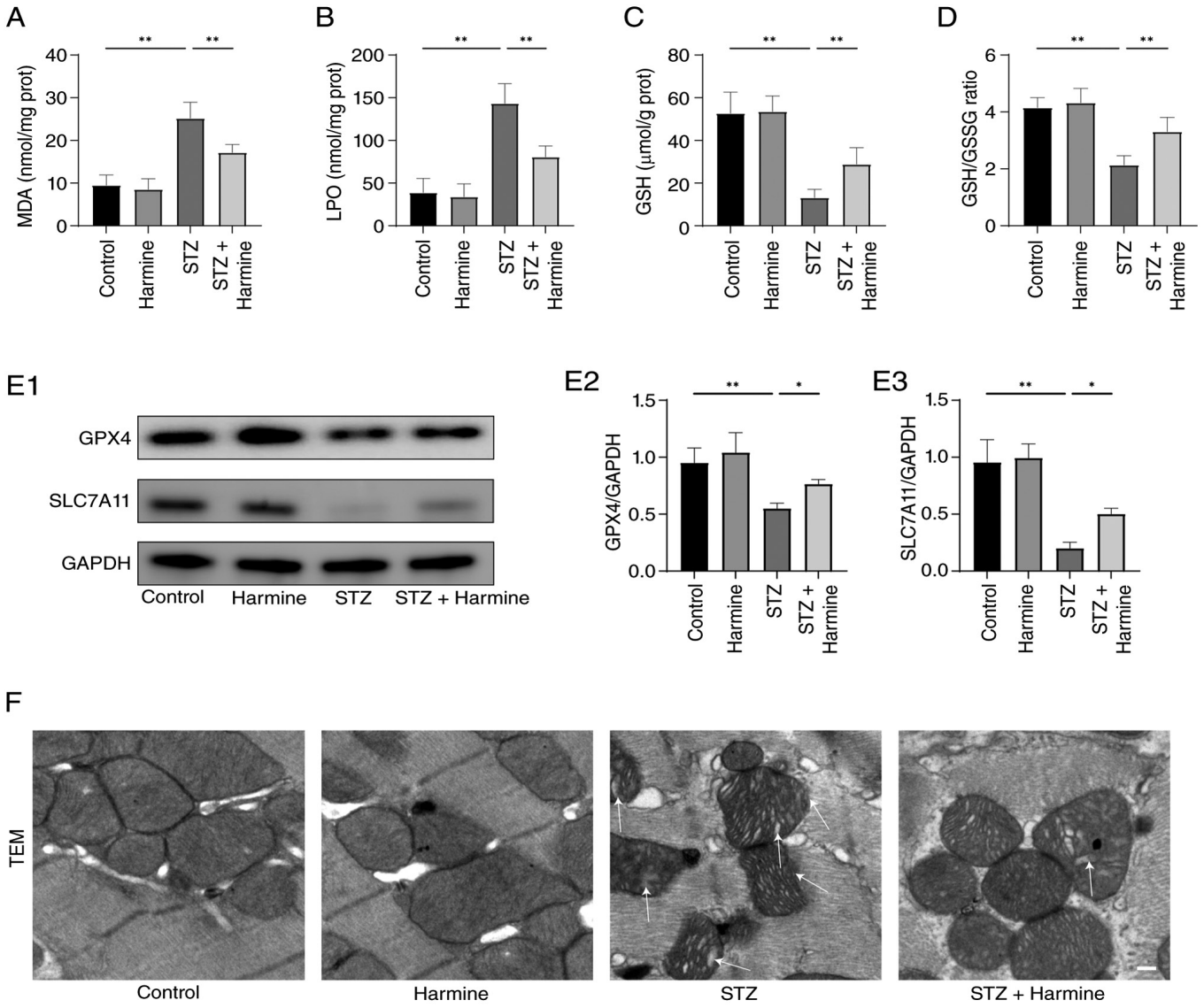

Figure 3. Inhibition of Dyrk1a ameliorates ferroptosis in type 1 diabetic mice. The levels of (A) MDA, (B) LPO, (C) GSH and (D) the GSH/GSSH ratio in cardiac tissue lysates were assessed in four groups of mice (n=6 for each group). (E) Representative (E1) western blots and quantitative data on the protein levels of (E2) GPX4 and (E3) SLC7A11 (n=4 per group). (F) Representative TEM images of mitochondrial morphology of cardiac tissue. The arrows indicate damaged mitochondria with cristae disruption and altered membrane density. Scale bar, 200 nm. Data are mean ± SD. *P<0.05, **P<0.01. Data were analyzed by using one-way ANOVA followed by Dunnett's post hoc test. STZ, streptozotocin, MDA, malondialdehyde, LPO, lipid peroxides, GSH, reduced glutathione, GSSG, oxidized glutathione, GPX4, glutathione peroxidase 4, SLC7A11, solute carrier family 7 member 11, TEM, transmission electron microscopy.

As demonstrated by substantiation from T1DM studies, autophagy suppression activates Nrf2-regulated ferroptosis pathways in cardiomyocytes, accelerating DCM progression (39). Conversely, Wang *et al* (9) put forth a viewpoint that Nrf2-activating sulforaphane prevents myocardial dysfunction in T2DM by upregulating ferritin/xCT to suppress ferroptosis. Collectively, these findings suggested ferroptosis inhibition as a promising therapeutic intervention against late-stage DCM. Although glucotoxicity and lipotoxicity are frequently underlined in T2DM, persistent hyperglycemia in T1DM can also trigger overlapping oxidative stress and ferroptosis-related pathways, thereby providing a relevant mechanistic context for the present study.

Therefore, the present study subsequently examined Dyrk1a, a kinase implicated in diverse pathologies comprising dementia, diabetes and cardiovascular disorders (40). Notably, this enzyme exhibits remarkable myocardial expression beyond neural tissues (16,41,42). As the present study suggested, DCM, a critical complication of T1DM, features substantially elevated Dyrk1a mRNA levels in cardiac tissue, suggesting its pathogenic involvement in diabetic heart injury. By employing Dyrk1a inhibitors, functional studies demonstrated cardioprotective effects. In detail, cellular viability compromised by hyperglycemia was restored, while ferroptosis markers showed noticeable attenuation. This manifested through decreased lipid peroxidation (MDA reduction) and ROS suppression, alongside increased GSH elevation. Corresponding molecular analyses revealed upregulated expression of ferroptosis-inhibitory proteins GPX4 and SLC7A11. Despite the fundamental fact that prior research linked Dyrk1a to ferroptosis in myocardial ischemia-reperfusion injury (43), its role in DCM

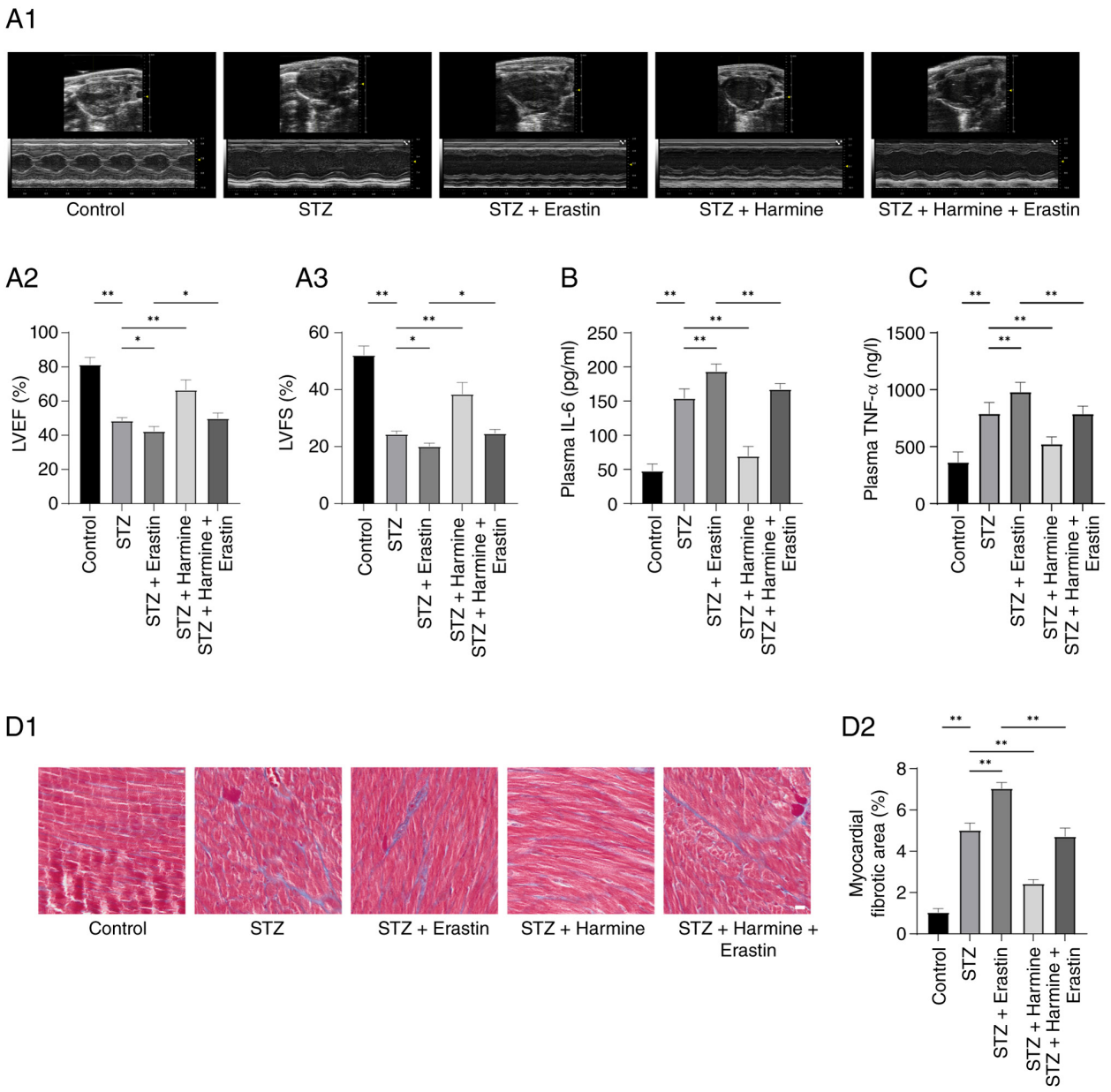

Figure 4. Erastin abolishes the protective effect of Harmine on diabetic cardiomyopathy. Type 1 diabetic mice received Harmine (12.5 mg/kg/day, intragastrically) either alone or in combination with the ferroptosis inducer erastin (40 mg/kg/day, administered intraperitoneally for three consecutive days). (A) Echocardiography was performed to assess cardiac function, encompassing (A1) representative M-mode imaging, (A2) left ventricular ejection fraction (LVEF%) and (A3) left ventricular fractional shortening (LVFS%) (n=6 for each group). Serum levels of inflammation-associated biomarkers, specifically (B) IL-6 and (C) TNF-α, were quantified (n=6 for each group). (D) Representative (D1) Masson staining images and (D2) quantification of the fibrotic areas. Scale bar, 10 μm. (n=6 for each group). Data are mean ± SD. *P<0.05, **P<0.01. Data were analyzed by employing one-way ANOVA followed by Tukey's post-hoc test. STZ, streptozotocin; LVEF, left ventricular ejection fraction; LVFS, left ventricular fractional shortening; IL-6, interleukin-6; TNF-α, tumor necrosis factor-α.

remained unexplored. As shown by the *in vivo* experiments, Dyrk1a suppression improved cardiac functional parameters and alleviated myocardial histopathological damage while concurrently inhibiting ferroptosis pathways. Crucially, the Class 1 ferroptosis inducer erastin, which depletes GSH synthesis by blocking cystine import via XC^- transport (44), abolished these therapeutic benefits in T1DM models (45), thereby confirming the mechanistic dependency on ferroptosis regulation. In control T1DM mice, erastin administration further aggravated cardiac injury, indicating that erastin may exert compounding toxicity in the diabetic heart. To sum up, these findings demonstrated that Dyrk1a inhibition attenuated DCM progression through targeted suppression of cardiomyocyte ferroptosis, positioning it as a promising therapeutic strategy for diabetic cardiac complications.

As the predominant Dyrk1a inhibitor among β-carboline alkaloids, harmine competitively blocks ATP binding within the kinase's catalytic pocket to suppress enzymatic activity. As well as its documented therapeutic spectrum, encompassing glioblastoma growth inhibition (46), cognitive improvement (47), adult human β-cell regeneration (48) and attenuation of cardiovascular pathologies (atherosclerosis and cardiac hypertrophy) (49,50), the present study demonstrated its striking cardioprotective efficacy against heart

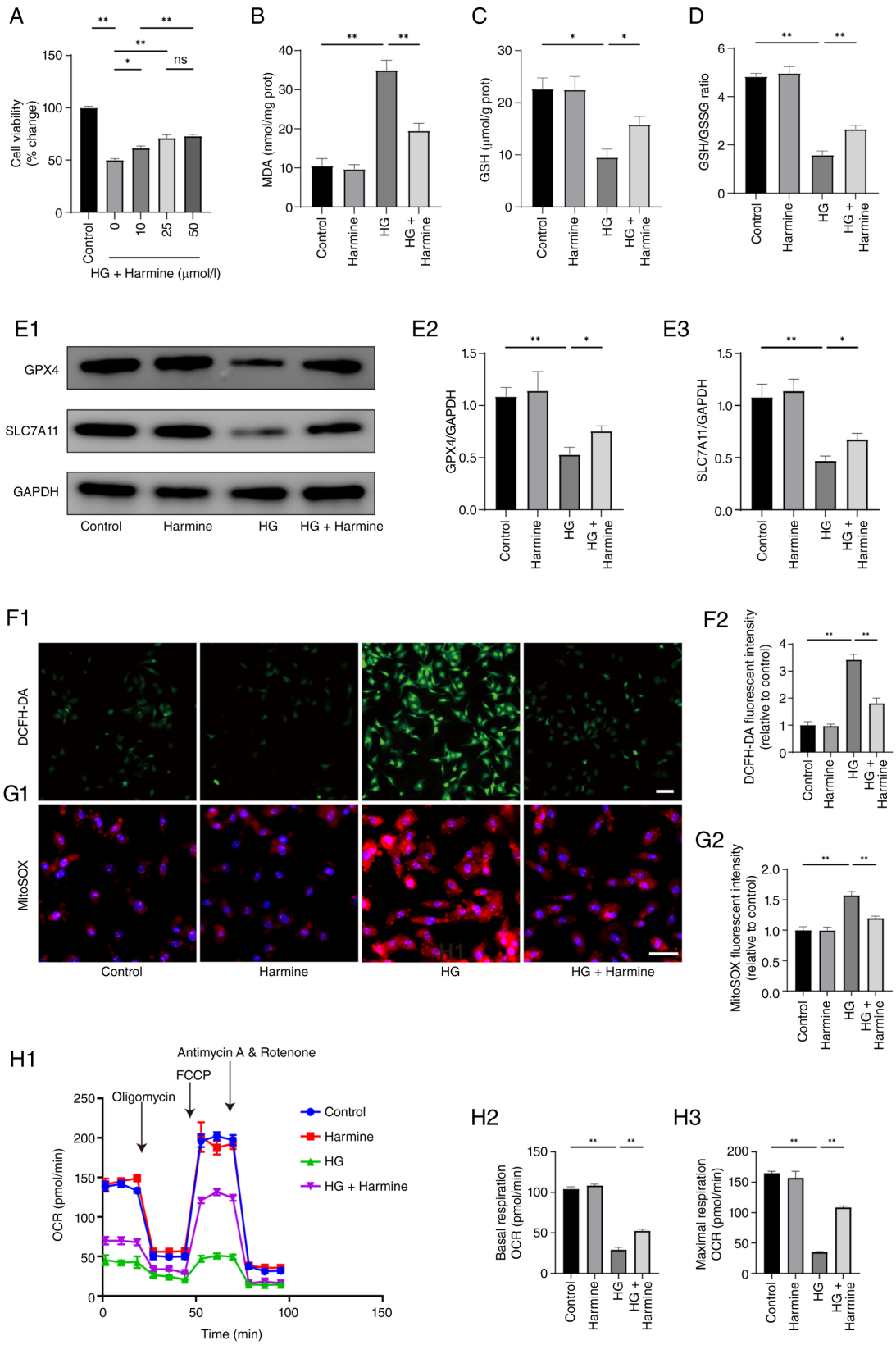

Figure 5. Harmine inhibits high glucose-induced cardiomyocyte injury and ferroptosis. Primary cardiomyocytes were incubated with HG (35 mmol/l) for 24 h in the presence or absence of Harmine (25 μmol/l) before assessment. (A) Primary cardiomyocyte viability was assessed by utilizing the CCK-8 assay (n=6 per group). (B) MDA (C), GSH and (D) GSH/GSSG ratio were quantified in primary cardiomyocytes by employing assay-specific kits (n=6 per group). (E1) Representative western blots and quantitative data on the protein levels of (E2) GPX4 and (E3) SLC7A11 (n=4 per group). (F) Images representing the fluorescence probe (F1) for ROS obtained from primary cardiomyocytes, accompanied by (F2) quantification. Scale bar, 100 μm. (n=6 for each group). (G) Representative (G1) MitoSOX-stained images and corresponding (G2) quantification of ROS levels. Scale bar, 50 μm. (n=6 for each group). (H) OCR in mitochondria of primary cardiomyocytes. (H1) Image representation along with quantification of (H2) basal respiration and (H3) maximum respiration. (n=5 in each group). Data are mean ± SD. *P<0.05, **P<0.01. Data were analyzed by one-way ANOVA followed by (A) Tukey's post-hoc test and (B-F) Dunnett's post hoc test. HG, high glucose; MDA, malondialdehyde; GSH, reduced glutathione; GSSG, oxidized glutathione; GPX4, glutathione peroxidase 4; SLC7A11, solute carrier family 7 member 11; ROS, reactive oxygen species; OCR, oxygen consumption rate.

failure progression in type 1 diabetic cardiomyopathy. These collective findings substantiated the translational promise of targeting Dyrk1a for cardiac repair applications.

Nevertheless, harmine is not fully selective for Dyrk1a and may also inhibit MAO-A, so off-target effects cannot be excluded. The present study did not validate the findings with a second Dyrk1a inhibitor or genetic knockdown. For this reason, further studies are indispensable to confirm the Dyrk1a-specific role in cardioprotection.

Altogether, the present study suggested that harmine may serve as a lead compound for the treatment of type 1 diabetic cardiomyopathy.

Acknowledgements

Not applicable.

Funding

The present study was supported in part by grants from the Science-Health Joint Medical Scientific Research Project of Chongqing (grant no. 2024QNXM030) and 2023 key Disciplines On Public Health Construction in Chongqing.

Availability of data and materials

The data generated in the present study may be requested from the corresponding author.

Authors' contributions

JC and WZ conceived and designed the study. JC, TH, JW and CC performed the experiments and analyzed the data. MH, JH, YZ and NY made substantial contributions to data interpretation, manuscript revision and supervision. JC and NY drafted the manuscript and revised it critically with feedback from all authors. MH, JH, JC and NY confirm the authenticity of all the raw data. All authors read and approved the final version of the manuscript.

Ethics approval and consent to participate

The animal experiments were approved by the ethical committee of Chongqing University (approval no. 2505001).

Patient consent for publication

Not applicable.

Competing interests

The authors declare that they have no competing interests.

References

1. Tauschmann M and Hovorka R: Technology in the management of type 1 diabetes mellitus-current status and future prospects. Nat Rev Endocrinol 14: 464-475, 2018.
2. Miki T, Yuda S, Kouzu H and Miura T: Diabetic cardiomyopathy: Pathophysiology and clinical features. Heart Fail Rev 18: 149-166, 2013.
3. Wei J, Zhao Y, Liang H, Du W and Wang L: Preliminary evidence for the presence of multiple forms of cell death in diabetes cardiomyopathy. Acta Pharm Sin B 12: 2021.
4. Wang X, Pan J, Liu D, Zhang M, Li X, Tian J, Liu M, Jin T and An F: Nicorandil alleviates apoptosis in diabetic cardiomyopathy through PI3K/Akt pathway. J Cell Mol Med 23: 5349-5359, 2019.
5. Tan Y, Zhang Z, Zheng C, Wintergerst KA, Keller BB and Cai L: Mechanisms of diabetic cardiomyopathy and potential therapeutic strategies: Preclinical and clinical evidence. Nat Rev Cardiol 17: 585-607, 2020.
6. Dixon SJ, Lemberg KM, Lamprecht MR, Skouta R, Zaitsev EM, Gleason CE, Patel DN, Bauer AJ, Cantley AM, Yang WS, *et al*: Ferroptosis: An iron-dependent form of nonapoptotic cell death. Cell 149: 1060-1072, 2012.
7. Jiang X, Stockwell BR and Conrad M: Ferroptosis: Mechanisms, biology and role in disease. Nat Rev Mol Cell Biol 22: 266-282, 2021.
8. Ni T, Huang X, Pan S and Lu Z: Inhibition of the long non-coding RNA ZFAS1 attenuates ferroptosis by sponging miR-150-5p and activates CCND2 against diabetic cardiomyopathy. J Cell Mol Med 25: 9995-10007, 2021.
9. Wang X, Chen X, Zhou W, Men H, Bao T, Sun Y, Wang Q, Tan Y, Keller BB, Tong Q, *et al*: Ferroptosis is essential for diabetic cardiomyopathy and is prevented by sulforaphane via AMPK/NRF2 pathways. Acta Pharm Sin B 12: 708-722, 2021.
10. Li W, Li W, Leng Y, Xiong Y and Xia Z: Ferroptosis is involved in diabetes myocardial Ischemia/Reperfusion injury through endoplasmic reticulum stress. DNA Cell Biol 39: 210-225, 2019.
11. Kay LJ, Smulders-Srinivasan TK and Soundararajan M: Understanding the multifaceted role of human down syndrome kinase DYRK1A. Adv Protein Chem Struct Biol 105: 127-171, 2016.
12. Aranda S, Laguna A and de la Luna S: DYRK family of protein kinases: Evolutionary relationships, biochemical properties, and functional roles. FASEB J 25: 449-462, 2010.
13. Wang L, Ouyang S, Li B, Wu H and Wang F: GSK-3β manipulates ferroptosis sensitivity by dominating iron homeostasis. Cell Death Discov 7: 334, 2021.
14. Wang Z, Yao M, Jiang L, Wang L, Yang Y, Wang Q, Qian X, Zhao Y and Qian J: Dexmedetomidine attenuates myocardial ischemia/reperfusion-induced ferroptosis via AMPK/GSK-3β/Nrf2 axis. Biomed Pharmacother 154: 113572, 2022.
15. Hille S, Dierck F, Kühl C, Sosna J, Adam-Klages S, Adam D, Lüllmann-Rauch R, Frey N and Kuhn C: Dyrk1a regulates the cardiomyocyte cell cycle via D-cyclin-dependent Rb/E2f-signalling. Cardiovasc Res 110: 381-394, 2016.
16. Lan C, Chen C, Qu S, Cao N, Luo H, Yu C, Wang N, Xue Y, Xia X, Fan C, *et al*: Inhibition of DYRK1A, via histone modification, promotes cardiomyocyte cell cycle activation and cardiac repair after myocardial infarction. EBioMedicine 82: 104139, 2022.
17. Young A, Bradley LA, Farrar E, Bilcheck HO, Tkachenko S, Saucerman JJ, Bekiranov S and Wolf MJ: Inhibition of DYRK1a enhances cardiomyocyte cycling after myocardial infarction. Circ Res 130: 1345-1361, 2022.
18. Kumar K, Man-Un Ung P, Wang P, Wang H, Li H, Andrews MK, Stewart AF, Schlessinger A and DeVita RJ: Novel selective thiadiazine DYRK1A inhibitor lead scaffold with human pancreatic β-cell proliferation activity. Eur J Med Chem 157: 1005-1016, 2018.
19. Luo W, Lin K, Hua J, Han J, Zhang Q, Chen L, Khan ZA, Wu G, Wang Y and Liang G: Schisandrin B attenuates diabetic cardiomyopathy by targeting MyD88 and inhibiting MyD88-Dependent inflammation. Adv Sci (Weinh) 9: e2202590, 2022.
20. Gong W, Zhang S, Chen Y, Shen J, Zheng Y, Liu X, Zhu M and Meng G: Protective role of hydrogen sulfide against diabetic cardiomyopathy via alleviating necroptosis. Free Radic Biol Med 181: 29-42, 2022.
21. Li X, Luo W, Tang Y, Wu J, Zhang J, Chen S, Zhou L, Tao Y, Tang Y, Wang F, *et al*: Semaglutide attenuates doxorubicin-induced cardiotoxicity by ameliorating BNIP3-Mediated mitochondrial dysfunction. Redox Biology 72: 103129, 2024.
22. Chen X, Li Y, Yuan X, Yuan W, Li C, Zeng Y, Lian Y, Qiu X, Qin Y, Zhang G, *et al*: Methazolamide attenuates the development of diabetic cardiomyopathy by promoting β-Catenin degradation in type 1 diabetic mice. Diabetes 71: 795-811, 2022.

23. Livak KJ and Schmittgen TD: Analysis of relative gene expression data using real-time quantitative PCR and the 2(-Delta Delta C(T)) method. Methods 25: 402-408, 2001.
24. Lu QB, Ding Y, Liu Y, Wang ZC, Wu YJ, Niu KM, Li KX, Zhang JR and Sun HJ: Metrnl ameliorates diabetic cardiomyopathy via inactivation of cGAS/STING signaling dependent on LKB1/AMPK/ULK1-mediated autophagy. J Adv Res 51: 161-179, 2022.
25. Rajesh M, Bátkai S, Kechrid M, Mukhopadhyay P, Lee WS, Horváth B, Holovac E, Cinar R, Liaudet L, Mackie K, *et al*: Cannabinoid 1 receptor promotes cardiac dysfunction, oxidative stress, inflammation, and fibrosis in diabetic cardiomyopathy. Diabetes 61: 716-727, 2012.
26. Tan X, Hu L, Shu Z, Chen L, Li X, Du M, Sun D, Mao X, Deng S, Huang K and Zhang F: Role of CCR2 in the development of Streptozotocin-Treated diabetic cardiomyopathy. Diabetes 68: 2063-2073, 2019.
27. Raish M, Ahmad A, Bin Jardan YA, Shahid M, Alkharfy KM, Ahad A, Ansari MA, Abdelrahman IA and Al-Jenoobi FI: Sinapic acid ameliorates cardiac dysfunction and cardiomyopathy by modulating NF-κB and Nrf2/HO-1 signaling pathways in streptozocin induced diabetic rats. Biomed Pharmacother 145: 112412, 2021.
28. Abukhalil MH, Althunibat OY, Aladaileh SH, Al-Amarat W, Obeidat HM, Al-Khawalde AAA, Hussein OE, Alfwuaires MA, Algefare AI, Alanazi KM, *et al*: Galangin attenuates diabetic cardiomyopathy through modulating oxidative stress, inflammation and apoptosis in rats. Biomed Pharmacother 138: 111410, 2021.
29. Fang X, Ardehali H, Min J and Wang F: The molecular and metabolic landscape of iron and ferroptosis in cardiovascular disease. Nat Rev Cardiol 20: 7-23, 2023.
30. Zhao Y, Pan B, Lv X, Chen C, Li K, Wang Y and Liu J: Ferroptosis: Roles and molecular mechanisms in diabetic cardiomyopathy. Front Endocrinol (Lausanne) 14: 1140644, 2023.
31. Gan B: Mitochondrial regulation of ferroptosis. J Cell Biol 220: e202105043, 2021.
32. Li J, Jia YC, Ding YX, Bai J, Cao F and Li F: The crosstalk between ferroptosis and mitochondrial dynamic regulatory networks. Int J Biol Sci 19: 2756-2771, 2023.
33. Stockwell BR, Friedmann Angeli JP, Bayir H, Bush AI, Conrad M, Dixon SJ, Fulda S, Gascón S, Hatzios SK, Kagan VE, *et al*: Ferroptosis: A regulated cell death nexus linking metabolism, redox biology, and disease. Cell 171: 273-285, 2017.
34. Berdoukas V, Coates TD and Cabantchik ZI: Iron and oxidative stress in cardiomyopathy in thalassemia. Free Radic Biol Med 88: 3-9, 2015.
35. Fang X, Wang H, Han D, Xie E, Yang X, Wei J, Gu S, Gao F, Zhu N, Yin X, *et al*: Ferroptosis as a target for protection against cardiomyopathy. Proc Natl Acad Sci USA 116: 2672-2680, 2019.
36. Shirpoor A, Salami S, Khadem-Ansari MH, Ilkhanizadeh B, Pakdel FG and Khademvatani K: Cardioprotective effect of vitamin E: Rescues of diabetes-induced cardiac malfunction, oxidative stress, and apoptosis in rat. J Diabetes Complications 23: 310-316, 2008.
37. Huynh K, Kiriazis H, Du XJ, Love JE, Jandeleit-Dahm KA, Forbes JM, McMullen JR and Ritchie RH: Coenzyme Q10 attenuates diastolic dysfunction, cardiomyocyte hypertrophy and cardiac fibrosis in the db/db mouse model of type 2 diabetes. Diabetologia 55: 1544-1553, 2012.
38. Guo R, Liu W, Liu B, Zhang B, Li W and Xu Y: SIRT1 suppresses cardiomyocyte apoptosis in diabetic cardiomyopathy: An insight into endoplasmic reticulum stress response mechanism. Int J Cardiol 191: 36-45, 2015.
39. Zang H, Wu W, Qi L, Tan W, Nagarkatti P, Nagarkatti M, Wang X and Cui T: Autophagy inhibition enables Nrf2 to exaggerate the progression of diabetic cardiomyopathy in mice. Diabetes 69: 2720-2734, 2020.
40. Deboever E, Fistrovich A, Hulme C and Dunckley T: The omnipresence of DYRK1A in human diseases. Int J Mol Sci 23: 9355, 2022.
41. Hämmerle B, Ulin E, Guimera J, Becker W, Guillemot F and Tejedor FJ: Transient expression of Mnb/Dyrk1a couples cell cycle exit and differentiation of neuronal precursors by inducing p27KIP1 expression and suppressing NOTCH signaling. Development 138: 2543-2554, 2011.
42. Yang Y, Fan X, Liu Y, Ye D, Liu C, Yang H, Su Z, Zhang Y and Liu Y: Function and inhibition of DYRK1A: Emerging roles of treating multiple human diseases. Biochem Pharmacol 212: 115521, 2023.
43. Wang J, Xu RM, Cao QM, Ma BC, Zhang H and Hao HP: Mechanism of DYRK1a in myocardial ischemia-reperfusion injury by regulating ferroptosis of cardiomyocytes. Kaohsiung J Med Sci 39: 1190-1199, 2023.
44. Lillo-Moya J, Rojas-Solé C, Muñoz-Salamanca D, Panieri E, Saso L and Rodrigo R: Targeting ferroptosis against Ischemia/Reperfusion cardiac injury. Antioxidants (Basel) 10: 667, 2021.
45. Li X, Ma N, Xu J, Zhang Y, Yang P, Su X, Xing Y, An N, Yang F, Zhang G, *et al*: Targeting ferroptosis: Pathological mechanism and treatment of Ischemia-reperfusion injury. Oxid Med Cell Longev 2021: 1587922, 2021.
46. Pozo N, Zahonero C, Fernández P, Liñares JM, Ayuso A, Hagiwara M, Pérez A, Ricoy JR, Hernández-Laín A, Sepúlveda JM and Sánchez-Gómez P: Inhibition of DYRK1A destabilizes EGFR and reduces EGFR-dependent glioblastoma growth. J Clin Invest 123: 2475-2487, 2013.
47. Liu P, Li H, Wang Y, Su X, Li Y, Yan M, Ma L and Che H: Harmine ameliorates cognitive impairment by inhibiting NLRP3 inflammasome activation and enhancing the BDNF/TrkB signaling pathway in STZ-Induced diabetic rats. Front Pharmacol 11: 535, 2020.
48. Wang P, Karakose E, Liu H, Swartz E, Ackeifi C, Zlatanic V, Wilson J, González BJ, Bender A, Takane KK, *et al*: Combined inhibition of DYRK1A, SMAD and trithorax pathways synergizes to induce robust replication in adult human beta cells. Cell Metab 29: 638-652.e5, 2019.
49. Yang Y, Ma Q, Li Z, Wang H, Zhang C, Liu Y, Li B, Wang Y, Cui Q, Xue F, *et al*: Harmine alleviates atherogenesis by inhibiting disturbed flow-mediated endothelial activation via protein tyrosine phosphatase PTPN14 and YAP. Br J Pharmacol 178: 1524-1540, 2021.
50. Kuhn C, Frank D, Will R, Jaschinski C, Frauen R, Katus HA and Frey N: DYRK1A is a novel negative regulator of cardiomyocyte hypertrophy. J Biol Chem 284: 17320-17327, 2009.